Advances in Science and Technology Research Journal

Advances in Science and Technology Research Journal, 2026, 20(2), 470–479
https://doi.org/10.12913/22998624/211690
ISSN 2299-8624, License CC-BY 4.0

Received: 2025.10.15
Accepted: 2025.06.25
Published: 2025.12.23

Development of a Johnson-Cook constitutive model for 316L stainless steel manufactured by wire laser metal deposition

Radosław Kiciński[1]

[1] Mechanical – Electrical Department, Polish Naval Academy, ul. Śmidowicza 69, Gdynia, Poland
E-mail: r.kicinski@amw.gdynia.pl

ABSTRACT

Additive manufacturing (AM) of metals is increasingly used in engineering applications; however, the anisotropy of mechanical properties caused by the layer-by-layer deposition process poses challenges for constitutive modelling. This study focused on 316L stainless steel produced by wire laser metal deposition (WLMD) and aimed to develop a Johnson-Cook (J–C) constitutive model suitable for numerical simulations of this material. Tensile tests were performed on specimens printed in four build orientations (0°, 45°, 90°, and cross-directional XX), and the engineering stress-strain curves were converted into true stress-strain data. Young's modulus, yield strength ($Re_{0.2}$), ultimate tensile strength (UTS), and strain at UTS were determined for each orientation. The results demonstrated pronounced anisotropy: UTS ranged from ~610 MPa (90°) to ~660 MPa (0°), while total elongation varied between 28% and 37%, depending on the build direction. On the basis of on the true stress-strain data, simplified J–C parameters (A, B, n) were identified for each orientation, achieving a high quality of fit ($R^2 > 0.97$). The findings confirm that build orientation significantly influences the mechanical response of the WLMD-processed 316L, and that direction-dependent J–C parameters are necessary for reliable finite element (FE) simulations. The proposed model provides a foundation for more advanced constitutive descriptions, including strain-rate and temperature effects.

INTRODUCTION

Additive manufacturing is gaining importance across all industries. Currently, numerous technologies that enable the creation of prints from various materials are available on the market [1]. One of the additive manufacturing technologies is FDM (fused deposition modelling), which is widely used in scientific research due to its low cost and the ease of preparing prints for various experiments, particularly in the field of aerodynamics. The literature provides numerous examples of employing this technology to construct aircraft models for wind tunnel testing, including the Diamond DA42 [2], the South Korean FA-50 fighter aircraft [3], and the Italian M-346 Master trainer aircraft [4]. These models were designed in a CAD environment, then manufactured using FDM with PLA material, subjected to finishing treatments, and mounted on six-component aerodynamic balances. This approach enables the rapid and cost-effective preparation of research objects while maintaining adequate precision in geometry reproduction. FDM technology has also been applied to the fabrication of bluff body elements used in the studies on energy harvesting systems based on flow-induced vibrations [5]. Due to the simplicity of shaping and the flexibility in adjusting the mass and dimensions of the elements, a wide range of research configurations has been achieved. The cited examples confirm that 3D printing is becoming not only an alternative to classical methods of manufacturing models for experimental studies, but increasingly serves as a standard tool supporting the development of modern technologies in aviation and fluid engineering.

The authors of [6, 7] compared FDM/FFF with CNC machining for functional brackets, confirming significantly faster, low-waste production

and a more straightforward setup. However, printed PLA exhibits substantially lower dynamic stiffness than steel and typically requires minimal post-processing (e.g., drilling, threading), making it best suited for temporary, low-load service parts.

In recent years, there has been a dynamic development of additive technologies using metals, including the methods based on melting wire using heat sources, such as electric arcs, electron arcs, or laser beams. Particular interest is taken in 316L stainless steel, which, due to its corrosion resistance, good weldability, and stable mechanical properties, is one of the most commonly used materials in 3D printing. The literature contains analyses of the behaviour of this material under the conditions of intense thermal impact, e.g. during plasma atomisation [8], where the influence of rapid cooling and material fragmentation on the formation of structural inhomogeneities has been demonstrated.

According to the ASTM F2792 standard, metal additive manufacturing technologies are divided into powder bead fusion, directed energy deposition, binder jetting and sheet lamination. Powder metal printing is an expensive and inefficient technology. It involves a complex, physical and chemical metallurgical process that exhibits many types of heat and mass transfer, and in some cases, additional chemical reactions [9].

In connection with the above, another interesting direction of production is the use of welding wire. This approach allows for reducing printing costs and significantly increasing design possibilities. Depending on the type of energy used, this printing can be divided into three groups [10]: laser-based (WLMD), arc welding-based (WAAM) [11, 12], and electron beam forming (EBF) [13]. WAAM uses an electric arc as a heat source to melt the wire and form subsequent layers. The highest material deposition efficiency among wire methods characterises this technology. The process efficiency of up to 10 kg/h makes it cost-effective for large components. However, due to the low control over the arc, the influence of the deposition sequence and interlayer cooling results in worse geometry reproduction and part strength.

The second of the mentioned technologies is EBF. It is a NASA-patented method that utilises an electron beam in a vacuum environment to melt wire and produce metal components. It is mainly used in the aviation industry. EBF is characterised by the highest printing precision among wire methods, while maintaining a high deposition speed. Moreover, according to research [14], the prints are characterised by excellent mechanical properties, regardless of the process parameters. This method requires the process to be carried out in a vacuum chamber, which significantly increases the infrastructure costs. However, it is promising in the context of the space industry.

Wire and laser additive manufacturing (WLAM), utilising the WLMD technology, is a technique for additive metal production, where the energy source is a laser beam [15]. A typical WLAM system consists of a laser, an automatic wire feeder, a computerised numerical control (CNC) table or a robot arm, and auxiliary systems, such as a gas shield and a heating or cooling system. During the process, the laser generates a pool of liquid metal on the surface of the substrate, to which the wire is fed. The wire melts in the pool, creating a metallurgical connection with the substrate. The relative movement of the laser head and the wire feeder, in relation to the base material (or vice versa), results in the formation of successive paths and layers of material. This movement can be carried out by an industrial robot or a CNC table [16]. WLAM is characterised by great flexibility in the selection of materials – alloys based on iron, titanium and aluminium were tested. The Ti-6Al-4V alloy is of particular importance in this technology, as its mechanical properties and corrosion resistance found wide application in the aviation industry. The diameter of the wire used is usually in the range of 0.2 to 1.2 mm. The key aspects influencing the quality of the process include geometric accuracy, surface condition and mechanical properties of the deposited material (such as strength, hardness or residual stress level). These parameters are strongly dependent on both the properties of the wire (e.g., chemical composition, diameter) and the process conditions, such as the direction as well as angle of wire feeding, its speed, laser power, and welding speed. Currently, this technology uses infrared and blue lasers. The use of infrared (IR) and blue lasers (Blue Light) is associated with significant differences in the scope of radiation absorption, process efficiency, deposition quality and material compatibility. The choice of laser wavelength is crucial for the efficiency of wire melting and the quality of the deposited material, particularly in the cases involving highly reflective metals. The most commonly used are fibre lasers, which operate in

the infrared band (IR, approximately 1064 nm). However, blue lasers (wavelength 450–488 nm) are also used, especially in the context of materials such as copper or aluminium.

IR lasers are characterised by good absorption in titanium, nickel alloys, and steel. Still, their efficiency drops significantly in the case of reflective metals, such as copper and aluminium, where absorption is only a few per cent [17]. As a result, the process requires high power or special procedures, which increases energy losses and reduces the stability of the liquid metal pool.

In turn, blue lasers offer several times higher absorption in the visible range for materials such as copper (>60% at 450 nm), which translates into higher energy efficiency, lower radiation reflection and better process control [16]. In addition, blue lasers exhibit better beam concentration on a small surface, allowing for the precise melting of thin wires and the production of details with higher resolution.

As part of the everyday use of the above technology, the question arises about the strength of such parts in relation to the original. Numerous review articles in the literature describe a given technology, but there are relatively few publications on materials.

Many contemporary scholars are intensively researching metal additive manufacturing. The mechanical properties of 3D-printed titanium alloys [18,19] and various steels [20–22] have been widely investigated. A comprehensive review of the published data on the mechanical properties of metals produced by additive manufacturing methods (SLM, DMLS, EBM, DED) discusses the relationships between microstructure, defects, build orientation, post-processing, as well as their influence on tensile strength, fatigue, and hardness, as found in [23]. As emphasised in [24], the number of publications in this field has been growing exponentially.

The primary objective of this study was to develop a Johnson-Cook material model tailored explicitly to the stainless steel manufactured by WLMD, thereby enabling its direct application in numerical simulations. While numerous studies have focused on the mechanical characterisation of additively manufactured metals, including titanium alloys and stainless steels, existing constitutive models are predominantly derived for conventionally produced materials and rarely account for the anisotropy induced by additive manufacturing. The directional crystallographic texture formed during the WLMD process significantly influences the mechanical response of a material, creating a research gap in modelling its plastic behaviour. Addressing this issue, the present work proposes a Johnson-Cook model calibrated with the experimental data obtained for different deposition orientations, thus providing a more realistic and reliable representation of WLMD-processed steels in computational analyses.

MATERIALS AND METHODS

The tests used stainless steel type 316L, deposited using WLMD technology on an industrial Meltio M450 printer. This grade is characterised by high durability, low reactivity, and stable properties at elevated temperatures. Owing to its low carbon content, it is particularly recommended in the applications where there is a risk of intergranular corrosion [25]. The chemical composition and fundamental data of the 316L wire are presented in Table 1.

The printing process involved the layered deposition of the input material in the form of a wire, utilising an infrared laser beam as the energy source. The process parameters were as follows: layer height, 1 mm; line width, 1 mm; laser power, 1200 W; and deposition speed, 450 mm/min (7.5 mm/s). These values ensured stable path geometry and uniform microstructure, while the deposition was carried out under controlled environmental conditions. The samples were printed in four different directions relative to the central axis of the component structure: 0°, 45°, 90° and in the XX direction (default g-code). To better illustrate the sequence of steps and the deposition of successive layers, a schematic of the slicing strategy is provided (Figure 1). For comparison, reference samples were also prepared from rolled 316L steel. All samples had a rectangular cross-section, following the PN-EN ISO 6892-1:2020-05 standard (method B). With the 3D wire printing technology, these parts require appropriate post-printing processing. First of all, they must be cut off from the work table using a band saw or an EDM machine. Then they must be prepared for strength tests in accordance with the standard.

The tensile test was performed at ambient temperature (22±0.5 °C), according to the requirements of the standard. The tests were carried out on a Shimadzu AG-X plus testing machine using a contact extensometer.

Table 1. 316L welding wire basic data [16]

Wire chemical composition	Fe	C	Si	Mn	Cr	Ni	Mo
Weight percent	Balance	0.02	0.9	1.7	18.5	12.0	2.7
Wire density	8000 kg/m^3	Melting point	1671 K	Wire diameter	1.0 mm	Relative density	>99.7%

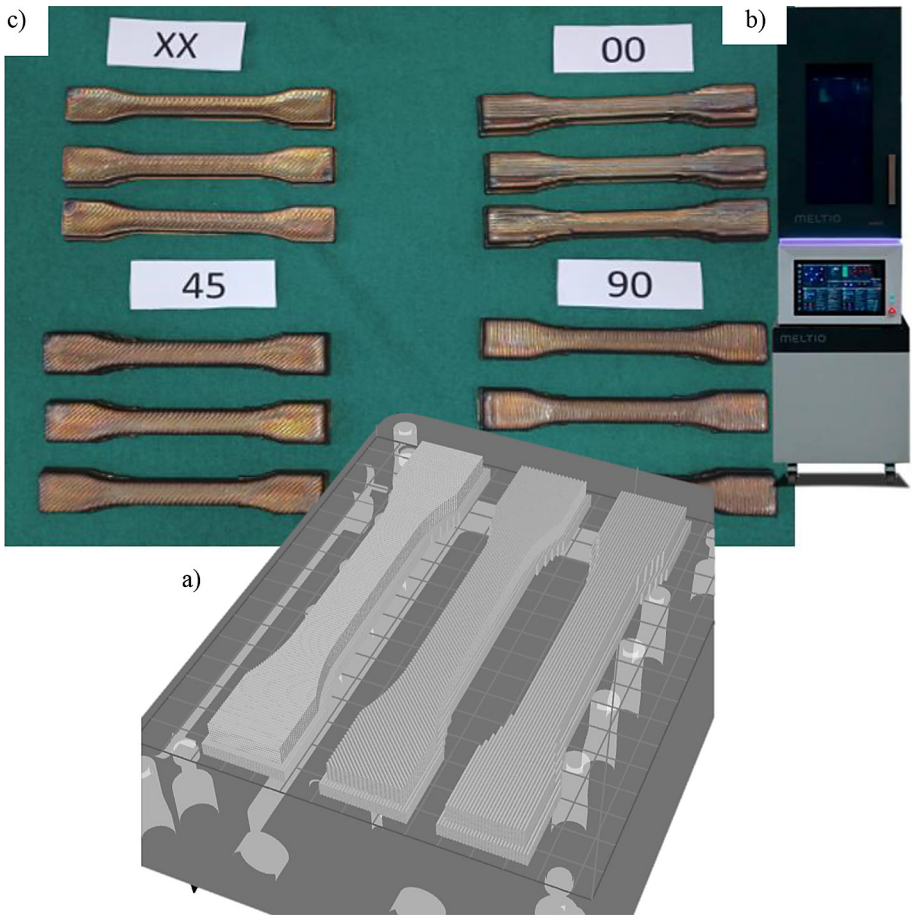

Figure 1. (a) WLMD 316L samples after printing and before machining; (b) Industrial Meltio M450 printer; (c) schematic view of the deposition strategy obtained from the slicing file

RESULTS

Three samples were tested for each group, and two samples were tested for the base material (Figure 2). The average for each group was then taken and presented in Figure 3.

Having the data from the testing machine, i.e. the so-called engineering curve, it is necessary to switch to true stresses. The relationship between the true stresses, s_{true} and nominal stresses s_{nom} obtained from the tensile test, is obtained assuming that the volume of the stretched sample during stretching is constant, so

$$l_0 \cdot A_0 = l \cdot A(F) \tag{1}$$

Hence:

$$\sigma_{\text{true}} = \frac{F}{A(F)} = \frac{F}{A_0}\frac{l}{l_0} = \sigma_{\text{nom}}\left(\frac{l}{l_0}\right) \tag{2}$$

Because:

$$\frac{l}{l_0} = 1 + \varepsilon_{\text{nom}} \tag{3}$$

$$\varepsilon_{\text{true}} = \ln(1 + \varepsilon_{\text{nom}}) \tag{4}$$

$$\sigma_{\text{true}} = \sigma_{\text{nom}}(1 + \varepsilon_{\text{nom}}) \tag{5}$$

So:

Plastic deformation is the difference between the true deformation e_{true}, and the elastic deformation e_{el}:

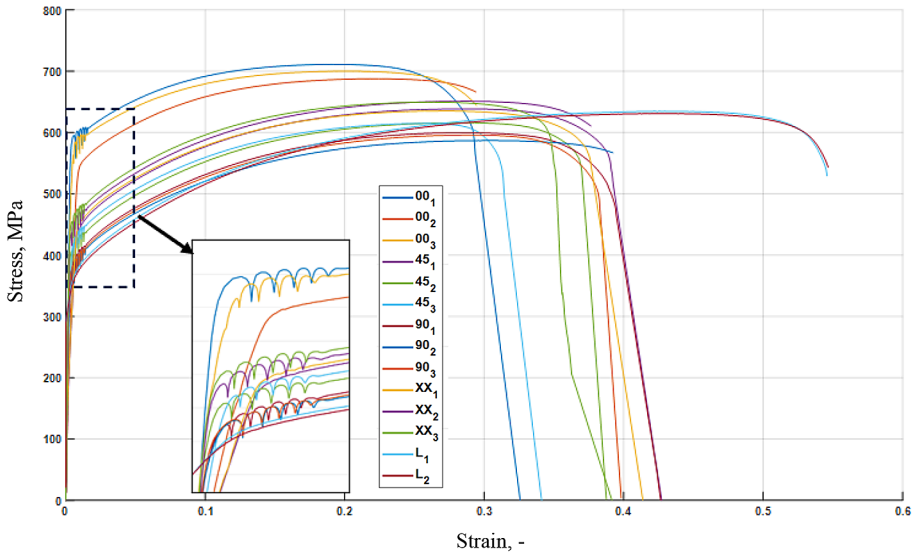

Figure 2. Summary of all tensile test results

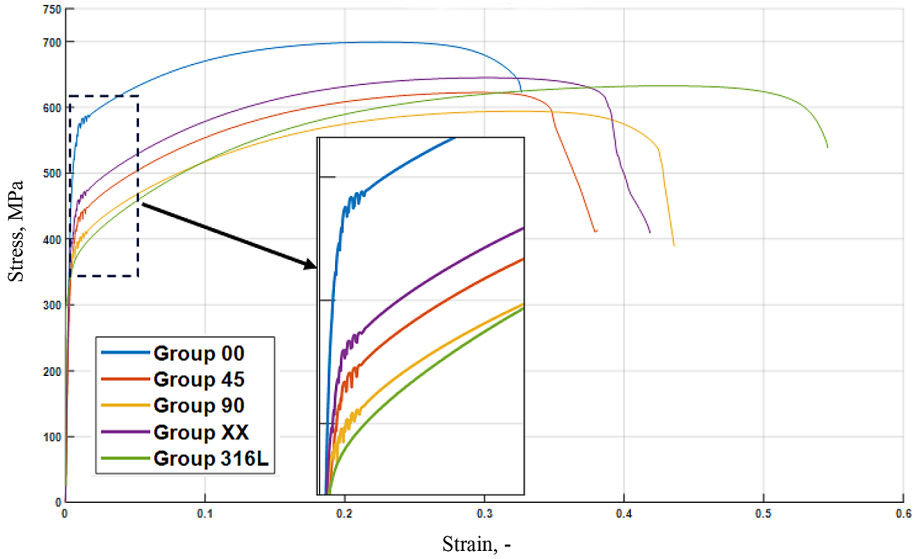

Figure 3. Average results from the tensile test for each group

$$\varepsilon_{\mathrm{pl}} = \varepsilon_{\mathrm{true}} - \varepsilon_{\mathrm{el}} = \varepsilon_{\mathrm{true}} - \frac{\sigma_{\mathrm{true}}}{E} \tag{6}$$

According to the above formulas, the true and plastic characteristics for the tested steel samples were developed. On the basis of the characteristics, the material data for each group were determined and presented in Table 2, while their summary is presented in Figure 4, 5.

In CAE programs, constitutive functions are employed to describe the plastic behaviour of materials, typically expressed as the true stress being a function of plastic strain, strain rate, and temperature: $\sigma_{\mathrm{true}} = \sigma_{\mathrm{true}}\left(\varepsilon_{\mathrm{pl}}, \dot{\varepsilon}, \theta\right)$. In the case of metals, the Johnson-Cook constitutive model has become the most frequently used standard [26–31]. In this model, the plastic Huber-Mises-Hencky (HMH) reduced stresses s_{pl} are described by the equation:

$$\sigma_{\mathrm{pl}} = \left(\mathrm{A} + \mathrm{B}\varepsilon_{\mathrm{pl}}^{n}\right)\left[1 + \mathrm{C}\ln\left(\frac{\dot{\varepsilon}}{\dot{\varepsilon}_0}\right)\right] \tag{7}$$

where: A – elastic range of the material $\sigma_{pl} = 0$ (it is often simplified in the form of $A=R_e$), B – hardening parameter, n – hardening exponent, C – strain rate coefficient, ε_{pl} – true plastic strain, $\dot{\varepsilon}$ – strain rate, $\dot{\varepsilon}_0$ – quasi-static strain rate (0.0001 s^{-1}), q – actual material temperature, q_0 – ambient

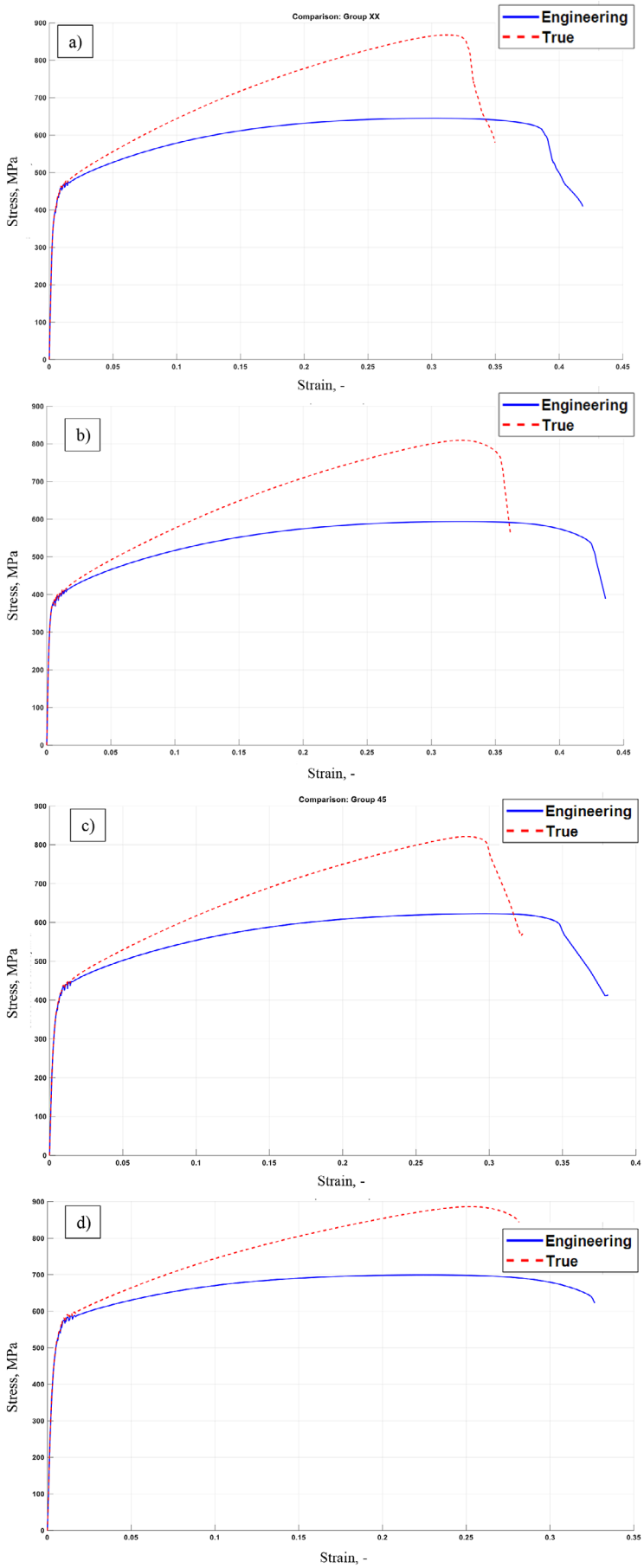

Figure 4. s_{true} -e_{pl} true characteristics for each group: a) group XX, b) group 00, c) group 90, d) group 45

Table 2. Material properties of individual groups

Group name	316L	XX	00	45	90
E (engineering), MPa	193000	151653	148182	131045	186434
Rm (engineering), MPa	633	645	699	622	594
Re02 (engineering), MPa	290	303	296	262	372
Strain at Rm	0.425	0.3008	0.2261	0.2979	0.3255
E (true), MPa	193000	151848	148373	131237	186644
Rm (true), MPa	935	867	886	821	809
Re02 (true), MPa	290	303	296	262	373

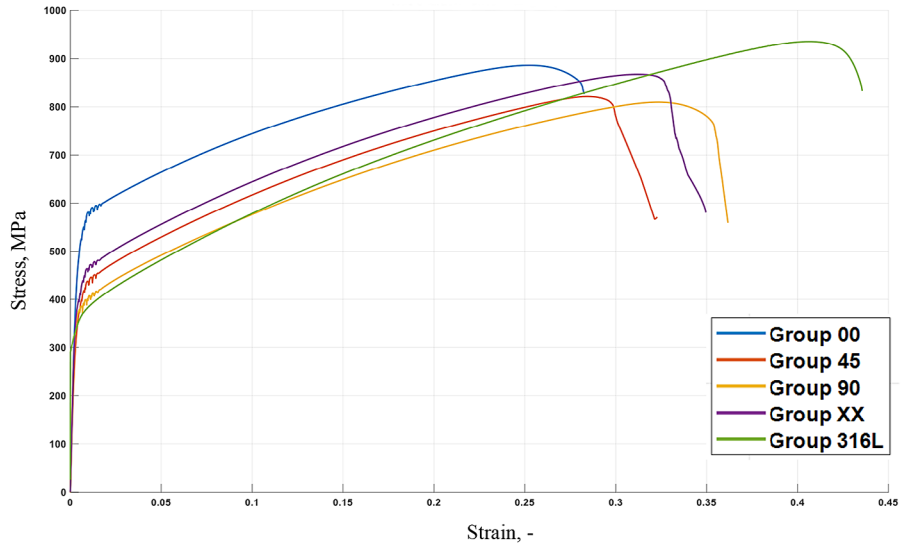

Figure 5. True stress–strain curves obtained from tensile tests for all specimen groups: 0°, 45°, 90°, XX (WLMD process), and reference rolled 316L steel (converted from engineering to true values ccording to standard relations)

temperature, q_{tmelt} – melting temperature, m – thermal softening exponent.

The values for this model presented above are determined based on the static tensile test and Hopkinson or Taylor tests [32].

The parameters *A, B, C, n* and *m* can be determined in many ways [33]. One of them is the so-called engineering formula, according to which the parameters of the first term, *A, B* and *n*, are determined based on the results of the static tensile test. In this case, it was decided to use the MATLAB environment, which used the code to fit the curve with the highest possible coefficient of determination (R^2). Using an appropriate script, the values of *A, B*, and *n* were determined, which are necessary to determine the simplified Johnson–Cook model. The values for each group are presented in Table 3, while the comparison of the model to the actual characteristics is presented in Figure 6.

DISCUSSION

The conducted tensile tests revealed significant differences between the printed samples and the reference rolled 316L steel. None of the stress-strain curves fully reproduced the behaviour of the conventional material. The additively manufactured specimens exhibited higher ultimate tensile strength but reduced plasticity, which can be attributed to the rapid solidification and local thermal cycling inherent in the WLMD process. These conditions lead to microstructural refinement, residual stresses, and the possible formation of crystallographic textures, which affect anisotropy.

A notable feature observed in all printed samples was distinct serrations on the stress-strain curves. This phenomenon likely indicates the occurrence of localised structural instabilities such as delamination at melt pool boundaries or incomplete fusion between successive layers. The

Table 3. Johnson-Cook model depending on printing direction

Direction	A, MPa	B, MPa	n	R^2
0_True	295	827	0.250	0.9762
45_True	262	931	0.398	0.9904
90_True	372	983	0.671	0.9966
XX_True	304	941	0.423	0.9935
316L_True	166	1145	0.429	0.9959

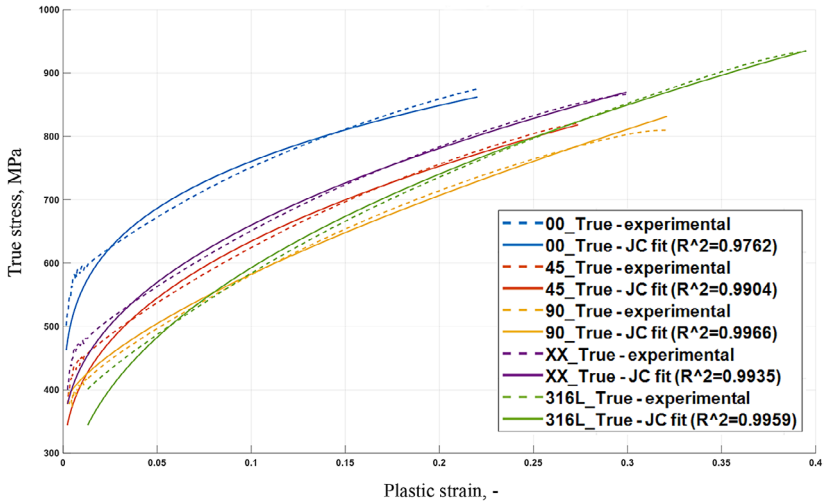

Figure 6. Comparison of the Johnson-Cook model with true characteristics

Table 4. Percentage differences of individual 3D printing material constants concerning the reference material

Group name	316L	XX	0	45	90
E (true), MPa	0.00%	21.32%	23.12%	32.00%	3.29%
R_m (true), MPa	0.00%	7.27%	5.24%	12.19%	13.48%
Re_{02} (true), MPa	0.00%	-4.48%	-2.07%	9.66%	-28.62%
Strain at R_m	0.00%	-29.22%	-46.8%	-29.91%	-23.41%

effect was particularly pronounced in the specimens printed at 45° and 90°, where interlayer bonding is more exposed to tensile loading.

Mechanical parameters, such as Young's modulus, yield strength, and ultimate tensile strength exhibited orientation-dependent variation (Table 4.). The most significant differences compared with the reference steel were noted for the modulus of elasticity (up to +32%) and strain at UTS (up to –46.8%), highlighting the strong anisotropy of WLMD material. These variations were successfully captured in the identified Johnson-Cook constitutive model, although the coefficients differ across build orientations. Despite this discrepancy, the obtained J–C models achieved a very good fit ($R^2 > 0.97$), confirming their applicability in CAE simulations.

CONCLUSIONS

The conducted research has demonstrated that the orientation of material deposition in WLMD significantly affects the mechanical properties of 316L stainless steel. All printed samples exhibited higher tensile strength compared to rolled 316L steel; however, this improvement came at the expense of reduced ductility, which may indicate increased brittleness and the influence of crystallographic transformations induced by laser-based solidification. Among the investigated orientations, the XX configuration, reflecting the natural deposition strategy, exhibited the mechanical properties most comparable to those of the reference material. However, it was still characterised by a lower modulus of elasticity and higher

strength. The appearance of distinct serrations on the stress–strain curves suggests the presence of local structural defects, such as delamination or incomplete fusion, emphasising the necessity of further optimisation of printing parameters. Simplified Johnson-Cook models were successfully calibrated for each printing orientation, with high quality of fit ($R^2 > 0.97$), confirming their suitability for use in numerical simulations provided that orientation-dependent anisotropy is considered. The obtained results underscore the significant potential of WLMD technology for producing large or complex components, particularly in the applications where rapid fabrication of replacement or temporary parts is required, such as in the aerospace, shipbuilding, and offshore industries. At the same time, the study indicated the need for future complementary microstructural investigations to verify the mechanisms underlying the observed anisotropy and serrated deformation behaviour.

Acknowledgements

This study was financed by the National Science Centre, Poland, under the MINIATURA programme (project no. 2024/08/X/ST11/00444, Development of mechanical properties of samples manufactured using Wire Laser Metal Deposition technology for numerical purposes). The work was corrected stylistically and linguistically using AI.

REFERENCES

1. Ding, D.; Pan, Z.; Cuiuri, D.; Li, H. Wire-feed additive manufacturing of metal components: technologies, developments and future interests. Int J Adv Manuf Technol 2015, 81, 465–481, https://doi.org/10.1007/s00170-015-7077-3
2. Domino, J.; Czyż, Z.; Bąbel, R. Aerodynamic Load Measurements on the Example of Diamond DA42 Model Aircraft. In Proceedings of the 2023 IEEE 10th International Workshop on Metrology for AeroSpace (MetroAeroSpace); IEEE: Milan, Italy, June 19 2023; 704–708.
3. Szatkowski, K.; Zahorski, T.; Czyż, Z. Measurements of Aerodynamic Loads on a Model of a Selected Fighter Aircraft. In Proceedings of the 2025 IEEE 12th International Workshop on Metrology for AeroSpace (MetroAeroSpace); IEEE: Naples, Italy, June 18 2025; 406–411.
4. Czyż, Z.; Karpiński, P.; Ruchała, P.; Zahorski, T. Preliminary Measurements for the Identification the Influence of the Test Object Support on the Aerodynamic Characteristics. In Proceedings of the 2024 11th International Workshop on Metrology for AeroSpace (MetroAeroSpace); IEEE: Lublin, Poland, June 3 2024; 399–404.
5. Karpiński, P.; Ambrożkiewicz, B.; Czyż, Z.; Litak, G. Performance analysis of piezoelectric energy harvesting system under varying bluff body masses and diameters – experimental study and validation with 0–1 test. Applied Sciences 2025, 15, 6972, https://doi.org/10.3390/app15136972
6. Jasiński, K.; Murawski, L.; Kluczyk, M.; Muc, A.; Szeleziński, A.; Muchowski, T.; Chodnicki, M. Selected aspects of 3D printing for emergency replacement of structural elements. Adv. Sci. Technol. Res. J. 2023, 17, 274–289, https://doi.org/10.12913/22998624/158486
7. Jasiński, K.; Murawski, L.; Kluczyk, M.; Wierzchowski, J.; Chodnicki, M.; Lipiński, K.; Szeleziński, A. Analysis of the possibility of using 3D printing for emergency replacement of damaged elements in the marine industry. Applied Sciences 2025, 15, 3458, https://doi.org/10.3390/app15073458
8. Gao, S.; Kryvtsun, I.; Korzhyk, V.; Strohonov, D.; Burlachenko, O.; Demianov, O.; Tereshchenko, O. Features of the process of formation and dispersion of a liquid layer and formation of powder particles in plasma-arc atomization of current-conducting solid and flux-cored wires. Adv. Sci. Technol. Res. J. 2025, 19, 58–72, https://doi.org/10.12913/22998624/201362
9. Gu, D.D.; Meiners, W.; Wissenbach, K.; Poprawe, R. Laser additive manufacturing of metallic components: materials, processes and mechanisms. International Materials Reviews 2012, 57, 133–164, https://doi.org/10.1179/1743280411Y.0000000014
10. Karunakaran, K.P.; Suryakumar, S.; Pushpa, V.; Akula, S. Low cost integration of additive and subtractive processes for hybrid layered manufacturing. Robotics and Computer-Integrated Manufacturing 2010, 26, 490–499, https://doi.org/10.1016/j.rcim.2010.03.008.
11. Le, V.T.; Banh, T.L.; Nguyen, D.T.; Le, V.T. Wire arc additive manufacturing of thin-wall low-carbon steel parts: microstructure and mechanical properties. Int. J. Mod. Phys. B 2020, 34, 2040154, https://doi.org/10.1142/S0217979220401542
12. Le, V.T.; Le, V.T. An Investigation on the Impact of the Interpass-Cooling Time on the Metallurgy of Wire-Arc-Additive-Manufacturing SS308L Components. In Proceedings of the 2nd Annual International Conference on Material, Machines and Methods for Sustainable Development (MMMS2020); Long, B.T., Kim, Y.-H., Ishizaki, K., Toan, N.D., Parinov, I.A., Vu, N.P., Eds.; Lecture Notes in Mechanical Engineering; Springer International Publishing: Cham, 2021; 196–201.

13. Strondl, A.; Fischer, R.; Frommeyer, G.; Schneider, A. Investigations of MX and Γ′/Γ″ Precipitates in the nickel-based superalloy 718 produced by electron beam melting. Materials Science and Engineering: A 2008, 480, 138–147, https://doi.org/10.1016/j.msea.2007.07.012
14. Taminger, K.M.B.; Hafley, R.A. Electron Beam Freeform Fabrication: A Rapid Metal Deposition Process 2003.
15. Sibisi, T.H.; Shongwe, M.B.; Tshabalala, L.C.; Mathoho, I. LAM additive manufacturing: a fundamental review on mechanical properties, common defects, dominant processing variables, and its applications. Int J Adv Manuf Technol 2023, 128, 2847–2861, https://doi.org/10.1007/s00170-023-12139-w
16. Technology – Wire-Laser Metal 3D Printing Available online: https://meltio3d.com/technology/ (accessed on 29 April 2025).
17. Zhao, C.; Fezzaa, K.; Cunningham, R.W.; Wen, H.; De Carlo, F.; Chen, L.; Rollett, A.D.; Sun, T. Real-time monitoring of laser powder bed fusion process using high-speed x-ray imaging and diffraction. Sci Rep 2017, 7, 3602, https://doi.org/10.1038/s41598-017-03761-2
18. Okuniewski W., Walczak M., Szala M., Chocyk D., Effect of surface modification by shot peening on cavitation erosion resistance of titanium alloy Ti-6Al-4V produced by DMLS method, Eng. Fail. Anal. 2025; 176: 109653. https://doi.org/10.1016/j.engfailanal.2025.109653
19. Gorsse, S.; Hutchinson, C.; Gouné, M.; Banerjee, R. Additive manufacturing of metals: a brief review of the characteristic microstructures and properties of steels, Ti-6Al-4V and high-entropy alloys. Sci Technol Adv Mater 2017, 18, 584–610, https://doi.org/10.1080/14686996.2017.1361305
20. Świetlicki, A.; Walczak, M.; Szala, M.; Nowak, W.J.; Chocyk, D. Effect of the shot peening finishing on cavitation erosion and corrosion resistance of DMLS manufactured 17-4PH steel. Engineering Failure Analysis 2025, 182, 110127, https://doi.org/10.1016/j.engfailanal.2025.110127
21. D'Andrea, D. Additive manufacturing of AISI 316L stainless steel: a review. Metals 2023, 13, 1370, https://doi.org/10.3390/met13081370
22. Sumanariu, C.A.; Amza, C.G.; Baciu, F.; Vasile, M.I.; Nicoara, A.I. Comparative analysis of mechanical properties: conventional vs. additive manufacturing for stainless steel 316L. Materials (Basel) 2024, 17, 4808, https://doi.org/10.3390/ma17194808
23. Lewandowski, J.J.; Seifi, M. Metal additive manufacturing: a review of mechanical properties. Annual Review of Materials Research 2016, 46, 151–186, https://doi.org/10.1146/annurev-matsci-070115-032024
24. Hosseini, E.; Popovich, V.A. A review of mechanical properties of additively manufactured Inconel 718. Additive Manufacturing 2019, 30, 100877, https://doi.org/10.1016/j.addma.2019.100877
25. Sawa, M.; Szala, M.; Henzler, W. Innovative device for tensile strength testing of welded joints: 3d modelling, fem simulation and experimental validation of test rig – a case study. Applied Computer Science 2021, 17, 92–105, https://doi.org/10.23743/acs-2021-24
26. Johnson, G.R.; Cook, W.H. A Constitutive Model and Data for Metals Subjected to Large Strains, High Strain Rates. Proceedings of the 7th International Symposium on Ballistics 2009.
27. Szturomski, B. Modelowanie Oddziaływania Wybuchu Podwodnego Na Kadłub Okrętu w Ujęciu Numerycznym [Modeling the Effect of the Underwater Explosion to Hull Board in a Numberic Concept – in Polish]; Akademia Marynarki Wojennej: Gdynia, 2016.
28. Szturomski, B. Inżynierskie Zastosowanie MES w Problemach Mechaniki Ciała Stałego Na Przykładzie Programu ABAQUS [Engineering Application of FEM in Problems of Solid Mechanics on the Example of the ABAQUS Program – Available in Polish]; Wydawnictwo Akademickie AMW: Gdynia, 2013.
29. Johnson G.R.; Stryk R.A; Beissel S.R. SPH for High Velocity Impact Computations. Computer Methods in Applied Mechanics and Engineering 1996.
30. Szturomski, B. Dynamic characteristics of high quality steel in johnson-cook's model for fast processes simulation in CAE programs. SSP 2015, 236, 31–38, https://doi.org/10.4028/www.scientific.net/SSP.236.31
31. Zhan, H.; Wang, G.; Kent, D.; Dargusch, M. Constitutive modelling of the flow behaviour of a β titanium alloy at high strain rates and elevated temperatures using the johnson–cook and modified Zerilli–Armstrong models. Materials Science and Engineering: A 2014, 612, 71–79, https://doi.org/10.1016/j.msea.2014.06.030
32. Korkmaz, M.E.; Verleysen, P.; Günay, M. Identification of constitutive model parameters for nimonic 80A superalloy. Trans Indian Inst Met 2018, 71, 2945–2952, https://doi.org/10.1007/s12666-018-1394-9
33. Flis L. Identyfikacja Parametrów Równania Konstytutywnego Johnsona-Cook'a w Odniesieniu Do Symulacji MES [Identification of Parameters of the Johnson-Cook Constitutive Equation for FEM Simulation – in Polish]. XIII Konferencji n.t. Techniki Komputerowe w Inżynierii 2014.